Journal of Computational Mathematics
Vol.28, No.5, 2010, 621–644.

http://www.global-sci.org/jcm
doi:10.4208/jcm.1001-m3006

# ADAPTIVE QUADRILATERAL AND HEXAHEDRAL FINITE ELEMENT METHODS WITH HANGING NODES AND CONVERGENCE ANALYSIS*

Xuying Zhao
*LSEC, ICMSEC, Academy of Mathematics and Systems Science, Chinese Academy of Sciences; and Graduate University of Chinese Academy of Sciences, Beijing 100190, China*
*Email: zhaoxy@lsec.cc.ac.cn*
Shipeng Mao and Zhong-Ci Shi
*LSEC, ICMSEC, Academy of Mathematics and Systems Science, Chinese Academy of Sciences, Beijing 100190, China*
*Email: maosp@lsec.cc.ac.cn shi@lsec.cc.ac.cn*

**Abstract**

In this paper we study the convergence of adaptive finite element methods for the general non-affine equivalent quadrilateral and hexahedral elements on 1-irregular meshes with hanging nodes. Based on several basic ingredients, such as quasi-orthogonality, estimator reduction and Döfler marking strategy, convergence of the adaptive finite element methods for the general second-order elliptic partial equations is proved. Our analysis is effective for all conforming $\mathbb{Q}_m$ elements which covers both the two- and three-dimensional cases in a unified fashion.

*Mathematics subject classification:* 65N12, 65N15, 65N30, 65N50, 35J25.
*Key words:* Finite element method, Adaptive algorithm, Hanging node, 1-irregular mesh, Convergence analysis.

## 1. Introduction

The adaptive finite element method (AFEM) is an efficient and reliable tool in the numerical solution of partial differential equations. The typical structure of the adaptive algorithm is made up of four modules: "Solve", "Estimate", "Mark", and "Refine". Even though adaptivity has been a fundamental tool of engineering and scientific computing for about three decades, the convergence analysis is rather recent. It started with Döfler [15], who introduced a crucial marking (from now on called Döfler's marking) and proved the strict energy reduction for the Laplacian provided the initial mesh $\mathcal{T}_0$ satisfies a fineness assumption. By introducing the concept of data oscillation and the interior node property, Morin *et al.* [21, 22] removed restriction on the initial mesh $\mathcal{T}_0$ and proved the convergence of AFEM. Very recently, Cascon *et al.* established the convergence of the self-adjoint second order elliptic problem without interior node property [9]. All of these results are based on an important tool, i.e., Galerkin-orthogonality. There are some results about nonstandard finite element methods in the literature. Carstensen and Hoppe proved the convergence of adaptive nonconforming and mixed finite element methods [7, 8]. One key ingredient of these papers is the so-called "quasi-orthogonality". This

* Received December 31, 2008 / Revised version received July 30, 2009 / Accepted November 6, 2009 / Published online May 1, 2010 /

technique is extended to the high order mixed finite element methods for the Poisson equation in [11]. So far, all the theoretical results have been limited to triangular or tetrahedral meshes.

The objective of this paper is to study the convergence of the adaptive conforming quadrilateral and hexahedral element methods. Since quadrilateral and hexahedral elements have been widely used in practical computing, it is important to study the adaptive algorithms for these general non-affine equivalent finite elements. As we know, local refinements on triangular or tetrahedral meshes are well developed, including newest-vertex-bisection, longest edge bisection and red-green refinement. However, the implementation of local refinement on quadrilateral and hexahedral meshes is, in some sense, more difficult than that on triangular or tetrahedral meshes. Nowadays, most researchers in the field of adaptive quadrilateral or hexahedral element methods use the so called 1-irregular mesh (see Section 3). By establishing some lemmas such as quasi-orthogonality, estimator reduction and so on, we finally prove the convergence of adaptive finite element methods on 1-irregular quadrilateral and hexahedral meshes for the general second-order elliptic partial equations, in which we can conquer the difficulties due to the non-affine mapping.

The rest of this paper is organized as follows. In the next section, we present the preliminary including the notation and the problem under consideration which is followed by the description of some concepts like shape regularity, hanging node and 1-irregular mesh. In Section 4, we prove the convergence of the corresponding adaptive algorithms. Since 1-irregular meshes are not conforming, the degrees of freedom on edges with hanging nodes must be constrained. The problem of how to assemble a symmetric positive definite stiff matrix will be discussed in Section 5 which also covers some numerical experiments. Conclusions will be presented in Section 6.

## 2. Problem and General Notations

Let $\Omega \in \mathbb{R}^d$ $(d \in \{2,3\})$ be a bounded, polyhedral domain with boundary $\Gamma := \partial\Omega$. We assume that the initial mesh $\mathcal{T}_0$ is a conforming quadrilateral or hexahedral partition of the domain $\Omega$. We consider a homogeneous Dirichlet boundary value problem for a linear second order elliptic partial differential equation(PDE):

$$\begin{cases} \mathcal{L}u := -\mathrm{div}(\mathbf{A}\nabla u) + \mathbf{b}\cdot\nabla u + cu = f, & \text{in } \Omega, \\ u = 0, & \text{on } \partial\Omega. \end{cases} \tag{2.1}$$

We assume

- $\mathbf{A} = (a_{ij})_{d\times d}$: $\Omega \mapsto \mathbb{R}^{d\times d}$ is symmetric positive definite and V-elliptic on $\Omega$ and $a_{ij} \in W^{1,\infty}(\Omega)(i,j = 1,2,\cdots,d)$;
- $\mathbf{b} = (b_k)_{d\times 1} \in (W^{1,\infty}(\Omega))^d$; $\quad c \in L^\infty(\Omega)$ and $c \geq 0$; $\quad f \in L^2(\Omega)$.

The weak formulation of (2.1) reads as follows: Find $u \in H_0^1(\Omega)$ such that

$$a(u,v) := (\mathbf{A}\nabla u, \nabla v) + (\mathbf{b}\cdot\nabla u, v) + (cu, v) = (f, v), \quad \forall v \in H_0^1(\Omega). \tag{2.2}$$

We denote by $\|\cdot\|_{a,\Omega}$ the energy norm

$$\|w\|_{a,\Omega}^2 := \int_\Omega \mathbf{A}\nabla w\cdot\nabla w + cw^2, \quad \forall w \in H_0^1(\Omega),$$

which is equivalent to the $H^1$ norm, i.e.,

$$c_a\|w\|_{1,\Omega} \le \|w\|_{a,\Omega} \le C_a\|w\|_{1,\Omega}, \quad \forall w \in H_0^1(\Omega). \tag{2.3}$$

By using the Cauchy-Schwarz inequality, one can easily show the continuity of the bilinear form $a(\cdot,\cdot)$, i.e.,

$$|a(w,v)| \le C_a\|w\|_{1,\Omega}\|v\|_{1,\Omega}, \quad \forall w, v \in H_0^1(\Omega).$$

Integrating by part leads to

$$\begin{aligned}\big|(\mathbf{b}\cdot\nabla v, v)\big| &= \big|\frac{1}{2}\int_\Omega \mathbf{b}\cdot\nabla(v^2)dx\big| = \big|-\frac{1}{2}\int_\Omega(\nabla\cdot\mathbf{b})v^2dx\big| \\ &\le \frac{\|\nabla\cdot\mathbf{b}\|_{0,\infty,\Omega}}{2}\|v\|_{0,\Omega}^2 \quad \forall v \in H_0^1(\Omega).\end{aligned}$$

Therefore, one can easily obtain the following Gårding's inequality

$$a(v,v) \ge \|v\|_{a,\Omega}^2 - \gamma_G\|v\|_{L^2(\Omega)}^2 \quad \forall v \in H_0^1(\Omega), \tag{2.4}$$

and

$$a(v,v) \le \|v\|_{a,\Omega}^2 + \gamma_G\|v\|_{L^2(\Omega)}^2 \quad \forall v \in H_0^1(\Omega), \tag{2.5}$$

where

$$\gamma_G = \frac{1}{2}\|\nabla\cdot\mathbf{b}\|_{0,\infty,\Omega}$$

is a constant.

We assume existence and uniqueness of the solution of (2.2) holds, which is equivalent to say, 0 is not the eigenvalue of the operator $\mathcal{L}$ by the Fredholm alternative theory (p. 303 in [16]). By the way, if $c > 0$, the existence and uniqueness of the solution of (2.2) follows from the maximum principle (p.124 in [18]). Note that if $\mathbf{b} = 0$, then the existence and uniqueness of the solution of (2.2) follows from Lax-Milgram theorem easily.

We use standard notations from Lebesgue and Sobolev space theory. For a measurable set $G \subset \Omega$, let $(\cdot,\cdot)_G$ and $\|\cdot\|_{0,G}$ denote the inner product and the norm in $L^2(G)$. We also use $(\cdot,\cdot)$ instead of $(\cdot,\cdot)_\Omega$ for simplicity. Furthermore, $|\cdot|_{m,G}$ and $\|\cdot\|_{m,G}$ denote the seminorm and norm in the Sobolev space $H^m(G)$ respectively. In particular, the associated seminorm $|\cdot|_{1,\Omega}$ on $H^1(\Omega)$ is actually a norm on

$$V := H_0^1(\Omega) = \Big\{v \in H^1(\Omega), v|_\Gamma = 0\Big\}.$$

We use $\mathcal{C}^n(G)$ to denote the space of all the $n$-times continuously differentiable functions, $\mathbb{P}_n(G)$ to denote the space of all polynomials of degree no more than $n$ and $\mathbb{Q}_n(G)$ to denote the space of degree no more than $n$ in each variable on the domain $G \subset \mathbb{R}^d$. By the way, if $E$ is an edge in $\mathbb{R}^d$ then $\mathbb{P}_m(E) = \mathbb{Q}_m(E)$ . For a compactly supported function $f$, $supp(f)$ denotes the compactly supported set of $f$. $\#J$ stands for the cardinal number of a finite set $J$. For a finite dimensional space $S$, we use $dim(S)$ to express the dimension of $S$. For a set $G \subset \mathbb{R}^d$, let $\overline{G}$ be the closure of $G$ and $|G|$ be the d-dimensional measure of $G$. Unless otherwise specified, a set $G \subset \Omega$ is an open set.

## 3. Shape Regularity, 1-irregular Mesh and Hanging Node

Let the bounded domain $\Omega \subset \mathbb{R}^d$ be decomposed by a mesh $\mathcal{T}_0$ of elements $K \in \mathcal{T}_0$ which are assumed to be open convex quadrilaterals in the 2D-case or open convex hexahedrons in the 3D-case such that $\overline{\Omega} = \cup_{K\in\mathcal{T}_0}\overline{K}$. In the 3D-case we also assume that each face of any hexahedral element in $\mathcal{T}_0$ is in a plane, i.e., we do not consider the case of a hexahedron with curved faces. Let $\mathcal{T}$ be a mesh generated by several times of a refinement from $\mathcal{T}_0$. For any element $K \in \mathcal{T}$, let $F_K : \hat{K} \to \overline{K}$ be the multilinear mapping between the reference element $\hat{K} := (-1, 1)^d$ and the original element $K$. Obviously, $F_K \in (\mathbb{Q}_1(\hat{K}))^d$. We follow the definition of shape regular mesh condition in the sense of [17] (p.105). Let $P_i$ $(1 \le i \le 2^d)$ be the vertex of any element $K \in \mathcal{T}$. We denote by $s_i$ the subtriangle with the vertex $P_i$ and two edges of $K$ containing $P_i$ as their one end in 2D-case or subtetrahedron with the vertex $P_i$ and three edges of $K$ containing $P_i$ as their one end in 3D-case (see Figure 3.1). Let $d_K$ be the diameter of $K$ and $\rho_i$ be the diameter or the largest ball inscribed in $s_i$. Define $\rho_K := \min_{1\le i\le 2^d} \rho_i$. We denote by $h_K = |K|^{\frac{1}{d}}$. Obviously,

$$\rho_K < h_K < \left(\frac{\pi}{6}\right)^{\frac{1}{d}} d_K.$$

**Definition 3.1 (Shape regularity)** *A mesh $\mathcal{T}$ is regular if there exists a constant $C_0 (C_0 > 1)$ such that*

$$\max_{K\in\mathcal{T}} \frac{d_K}{\rho_K} \le C_0. \tag{3.1}$$

Next we will describe the type of meshes treated in this paper. We assume that $\mathcal{T}$ is a *multilevel adaptive mesh* generated by a refinement process in the following way. We start with a regular partition $\mathcal{T}_0$ of the domain $\Omega$ into elements $K \in \mathcal{T}_0$ of mesh-level 0. The mesh $\mathcal{T}_0$ is assumed to be conforming, i.e., for any different elements $K_1,\ K_2 \in \mathcal{T}_0$, the intersection $\overline{K_1} \cap \overline{K_2}$ is either empty or a common $(d - m)$-dimensional face of $K_1$ and $K_2$ where $m \in \{1, \cdots, d\}$. Now, starting with the element $K \in \mathcal{T}_0$, an existing element $K$ can be split into $2^d$ new elements called *son-elements* of $K$ and denoted by $\mathcal{S}_i(K)$, $i = 1, \cdots, 2^d$, cf., Figure 3.1.

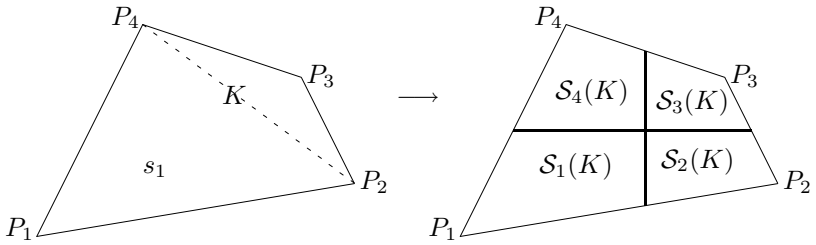


Fig. 3.1. (left) The subtriangle $s_1$ of element $K$; (right) Bisections on quadrilateral $K$ and son-elements $\mathcal{S}_i(K)$ of $K$, $i = 1, \cdots, 2^d$, $d = 2$.

These son-elements are constructed by connecting the barycenters of opposite $(d - 1)$-dimensional faces of $K$ and additionally, in the 3-dimensional case, by connecting the midpoints of opposite element edges in the 2-dimensional faces of $K$. For a new element $K' = \mathcal{S}_i(K)$, we will say that $K$ is the *father-element* of $K'$ and will write $K = \mathcal{F}(K')$. If an element $K$

is refined then, in the partition of the domain $\Omega$, it is replaced by the set of its son-elements $\mathcal{S}_i(K)$, $i = 1, \cdots, 2^d$. The new elements can be refined repeatedly and so the final partition $\mathcal{T}$ of $\Omega$ is created. Obviously, this local regular refinement is just the usual bisection and $\mathcal{T}$ satisfies the shape regular condition (3.1).

**Lemma 3.1.** *Let $\mathcal{T}$ be a shape regular mesh, then there exists a constant $\chi \in (0,1)$ such that*

$$\frac{|\mathcal{S}_i(K)|}{|K|} \leq \chi < 1 \quad \forall K \in \mathcal{T},\ i = 1, \cdots, 2^d. \tag{3.2}$$

*Proof.* Let $\alpha(d)$ be the measure of unit ball $B(0,1)$ in $\mathbb{R}^d$. Without loss of generality, we consider $\mathcal{S}_1(K)$ shown in Figure 3.1. Applying shape regular condition 3.1, one can get

$$|K| > |\mathcal{S}_1(K)| > \frac{1}{2^d}|s_1| > \frac{\alpha(d)}{2^d}\rho_K^d \geq \frac{\alpha(d)}{C_0^d 2^d} d_K^d > \frac{6\alpha(d)}{2^d C_0^d \pi}|K|.$$

Setting $C' := 6\alpha(d)/(2^d C_0^d \pi)$ leads to

$$\frac{|\mathcal{S}_i(K)|}{|\mathcal{S}_j(K)|} < \frac{1}{C'} \ \text{ for } \ i \neq j \text{ and } i, j = 1, \cdots, 2^d.$$

Summing over $j = 1, \cdots, 2^d$ yields

$$\frac{|\mathcal{S}_i(K)|}{|K|} < \frac{1}{1 + (2^d - 1)C'} := \chi < 1, \quad \forall K \in \mathcal{T},\ i = 1, \cdots, 2^d.$$

This completes the proof of the lemma. □

**Definition 3.2.** *For an element $K \in \mathcal{T}$, generated from the initial mesh $\mathcal{T}_0$ by the refinement process described above we define the* ***refinement level*** *$L(K)$ as $L(K) := 0$ if $K \in \mathcal{T}_0$ and $L(K) := m \geq 1$ if there exists a chain of $m$ father-elements $K_i$, $i = 1, \cdots, m$, starting from $K_0 := K$ and defined by*

$$K_i := \mathcal{F}(K_{i-1}) \text{ for } i = 1, \cdots, m,$$

*such that $K_m \in \mathcal{T}_0$.*

The above defined refinement level $L(K)$ is equal to the number of refinement steps that are needed to generate element $K$ from an element of the coarsest mesh $\mathcal{T}_0$.

**Definition 3.3.** *A mesh $\mathcal{T}$, which has generated by the above defined refinement process from a regular initial mesh $\mathcal{T}_0$, is called* ***k-irregular****($k \geq 0$ and $k \in \mathbb{Z}$) if*

$$|L(K) - L(K')| \leq k \tag{3.3}$$

*holds for any pair of neighbored elements $K,\ K' \in \mathcal{T}$ where $\partial K \cap \partial K'$ is a one- or two-dimensional manifold.*

Note that (3.3) need not be satisfied for pairs of element $K$, $K'$ having only one vertex in common. A 0-irregular mesh is a conforming mesh (without hanging nodes). Hereafter, we only consider 1-irregular meshes and the corresponding local refinement is described in Algorithm 3.1.

**Algorithm3.1** Local bisection refinement
Input: A 1-irregular mesh $\mathcal{T}_\ell$ with the set of marked elements $\mathcal{M}_\ell$ (If $\ell = 0$, then $\mathcal{T}_0$ is a conforming mesh).

1. Bisect all elements in $\mathcal{M}_\ell$ shown in Figure 3.1;
2. If there is a pair of two neighbored elements which do not satisfy (3.3) with $k = 1$, then bisect the element with lower refinement level.
3. Repeat step 2 until (3.3) holds with $k = 1$ for all pairs of neighbored elements in the current mesh.

Output: The refined 1-irregular mesh $\mathcal{T}_{\ell+1} = \text{REFINE}(\mathcal{T}_\ell, \mathcal{M}_\ell)$.

By the way, if we say $\mathcal{T}$ is shape regular, it means $\mathcal{T}$ is a 1-irregular multilevel adaptive mesh satisfying shape regularity (3.1). Next we will give the abstract definition of hanging nodes. Denote by $\mathcal{E}(K)$ the set of all $(d-1)$-dimensional faces of an element $K$. Let $\mathcal{E} := \bigcup_{K\in\mathcal{T}} \mathcal{E}(K)$ be the set of all element faces of the mesh. We split $\mathcal{E}$ as Fig.

$$\mathcal{E} = \mathcal{E}_0 \cup \mathcal{E}_\Gamma,$$

where $\mathcal{E}_\Gamma$ describes the set of all faces located at the boundary $\Gamma$ of $\Omega$ and $\mathcal{E}_0$ denotes the set of the inner faces of $\mathcal{E}$. For any face $E \in \mathcal{E}$, we define

$$\mathcal{T}(E) := \big\{K \in \mathcal{T} \mid E \in \mathcal{E}(K)\big\},$$

as the set of all elements having $E$ as one of their faces. Let $\mathcal{E}_r$ denote the set of the regular inner faces defined as

$$\mathcal{E}_r := \big\{E \in \mathcal{E}_0 \mid \#(\mathcal{T}(E)) = 2\big\}.$$

For each regular face $E \in \mathcal{E}_r$, there exist exactly two different elements denoted by $K(E)$ and $K'(E)$ such that $E$ is their common face, i.e.,

$$\mathcal{T}(E) := \big\{K(E),\ K'(E)\big\} \quad \forall E \in \mathcal{E}_r.$$

For all other faces $E \in \mathcal{E}\backslash\mathcal{E}_r$, there is only one element denoted by $K(E)$ which has $E$ as one of its faces, i.e.,

$$\mathcal{T}(E) := \big\{K(E)\big\} \quad \forall E \in \mathcal{E}\backslash\mathcal{E}_r.$$

A face $\tilde{E} \in \mathcal{E}$ is called a *son-face* of a face $E \in \mathcal{E}$ if $\tilde{E} \subset E$ and $|\tilde{E}| < |E|$ (see Fig. 3.2). We denote by $\mathcal{S}(E)$ the set of all son-faces of $E$. Note that for each regular face $E \in \mathcal{E}_r$, the set $\mathcal{S}(E)$ is empty. We define the set $\mathcal{E}_i$ of all *irregular inner faces* as

$$\mathcal{E}_i := \big\{E \in \mathcal{E}_0 \mid \mathcal{S}(E) \neq \emptyset\big\}.$$

Let $\tilde{E} \in \mathcal{S}(E)$ be a son-face of $E \in \mathcal{E}_i$, then the face $E$ is called the *father-face* of $\tilde{E}$ and we write $E = \mathcal{F}(\tilde{E})$. We define the set of all son-faces by

$$\mathcal{E}_s := \bigcup_{E\in\mathcal{E}_i} \mathcal{S}(E).$$

Using these definitions, the set $\mathcal{E}_0$ of all inner faces can be decomposed as

$$\mathcal{E}_0 = \mathcal{E}_r \cup \mathcal{E}_i \cup \mathcal{E}_s.$$

Let $\mathcal{N}(K)$ denote the vertices of any element $K \in \mathcal{T}$. Obviously, $\#\mathcal{N}(K) = 2^d$. The set of all nodes of the mesh $\mathcal{T}$ reads $\mathcal{N} := \sum_{K\in\mathcal{T}} \mathcal{N}(K)$.

**Definition 3.4.** *A node $A \in \mathcal{N}$ is called a **hanging node** if there exists a son-face $E \in \mathcal{E}_s$ such that*

$$A \in \overline{E} \quad \textit{and} \quad A \in \mathcal{N}(K(E))\backslash\mathcal{N}(K(\mathcal{F}(E))), \tag{3.4}$$

*where $K(E)$ and $K(\mathcal{F}(E))$ denote the uniquely determined elements associated with the face $E$ and its father-face $\mathcal{F}(E)$, respectively. A node $P \in \mathcal{N}$ is called a **regular node** if it is not a hanging node.*

The subset of $\mathcal{N}$ associated with the hanging nodes is denoted by $\mathcal{N}_h$ and $\mathcal{N}_r := \mathcal{N}\backslash\mathcal{N}_h$ denotes the set of all regular nodes. The corresponding local sets of regular and hanging nodes of an element $K \in \mathcal{T}$ are defined as

$$\mathcal{N}_h(K) := \mathcal{N}_h \cap \mathcal{N}(K) \text{ and } \mathcal{N}_r(K) := \mathcal{N}_r \cap \mathcal{N}(K).$$

A typical 2D-configuration with hanging node $A$ and associated regular nodes $A_1, A_2 \in \Lambda(A)$ is depicted in Figure 3.2. A node $A \in \mathcal{N}$ is a hanging node if there exists an element $K \in \mathcal{T}$ such that $A \in \partial K$ but $A$ is not a vertex of $K$. Furthermore, one can easily see the following characterization of a hanging node.

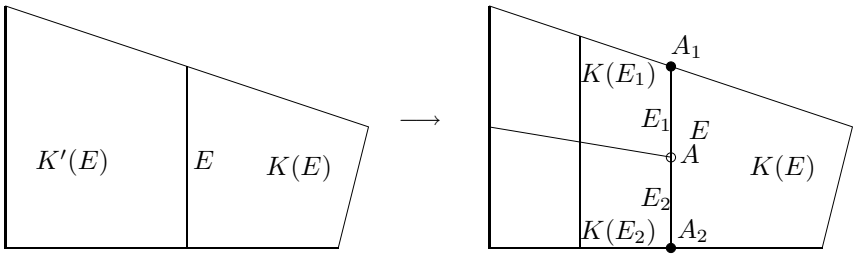


Fig. 3.2. (left) regular inner face $E \in \mathcal{E}_r$ with the two associated elements $K(E)$ and $K'(E)$; (right) irregular inner face $E \in \mathcal{E}_i$ with the son-faces $E_1,\ E_2 \in \mathcal{S}(E)$ where to each face only one element is associated and denoted by $K(E_1), K(E_2)$; (right) hanging node $A$ and associated regular nodes $A_1, A_2 \in \Lambda(A)$.

**Lemma 3.2.** *Let $\mathcal{T}$ be a 1-irregular mesh consisting of quadrilateral or hexahedral elements. Then a hanging node $A \in \mathcal{N}_h$ can be represented uniquely as a linear combination of some regular nodes in the following way*

$$A = \sum_{A_j\in\Lambda(A)} c(A)A_j \quad \textit{and} \quad \Lambda(A) \subset \mathcal{N}_r, \tag{3.5}$$

*where either*

$$\Lambda(A) := \{A_1, A_2\}, \quad c(A) = \frac{1}{2} \tag{3.6}$$

*and $A$ is the midpoint of an element edge $e$ with the two vertices $A_1$ and $A_2$ in the $2D$-case or $3D$-case, or*

$$\Lambda(A) := \{A_1, A_2, A_3, A_4\}, \quad c(A) = \frac{1}{4}, \tag{3.7}$$

*and $A$ is the barycenter of a two-dimensional face $E \in \mathcal{E}_i$ with the four vertices $A_1, A_2, A_3, A_4$ in the 3D-case.*

## 4. Convergence of AFEMs on 1-irregular Meshes

First, define the constrained approximation space with zero boundary as

$$V_{\mathcal{T}}^m := \left\{ v \in H_0^1(\Omega) : v|_K \circ F_K \in \mathbb{Q}_m(\hat{K}), \forall K \in \mathcal{T} \right\}, \tag{4.1}$$

where the degrees of freedom are taken with the usual Lagrange or Serendipity conforming finite element spaces and then give the discrete weak formulation of the problem (2.1) as: Find $u_{\mathcal{T}} \in V_{\mathcal{T}}^m$ such that

$$a(u_{\mathcal{T}}, v_{\mathcal{T}}) = (f, v_{\mathcal{T}}), \quad \forall\ v_{\mathcal{T}} \in V_{\mathcal{T}}^m. \tag{4.2}$$

The existence of $u_{\mathcal{T}}$ of the discrete problem (4.2) is obvious since $V_{\mathcal{T}}^m$ is a finite dimensional space. We only need to explain the uniqueness of $u_{\mathcal{T}}$. Schatz showed in [23] that the discrete problem has a unique solution for triangulations if the mesh-size $h$ is sufficiently small, i.e., $h \leq \tilde{h}$ for some constant $\tilde{h}$ depending on the shape regularity and data but not computable. The key of the proof is Gårding's inequality and Nitsche technique, which also holds for quadrilateral and hexahedral meshes including 1-irregular meshes. Hence we know that if $h_{\mathcal{T}} \leq \hbar$ for some constant $\hbar$ then the discrete problem (4.2) has a unique solution.

We need an $H^1$-interpolation operator like Clement-type or Scott-Zhang type interpolation operator on 1-irregular meshes, which can be found in [19]. Here we describe the interpolation operator in brief. Similar to Scott-Zhang [24], assign to each regular node $A_j \in \mathcal{N}_r$ a face $E_j \in \mathcal{E}_r \cup \mathcal{E}_i \cup \mathcal{E}_\Gamma$, such that the following conditions are satisfied:

$$\begin{aligned} &A_j \in \overline{E_j}\ , \\ &A_j \in \partial\Omega \Rightarrow E_j \subset \partial\Omega\ . \end{aligned}$$

For a regular node $A_j \in \mathcal{N}_r$, define the nodal functional $N_j : H^1(\Omega) \to \mathbb{R}$ by

$$N_j(v) := \frac{1}{|E_j|} \int_{E_j} v \mathsf{ds}, \quad \forall v \in H^1(\Omega),\ A_j \in \mathcal{N}_r.$$

For a hanging node $A_i \in \mathcal{N}_i$, define the nodal functional $\widetilde{N_i} : H^1(\Omega) \to \mathbb{R}$ as the following linear combination of nodal functionals for regular nodes

$$\widetilde{N_i}(v) := \sum_{A_j \in \Lambda(A_i)} c(A_i) N_j(v), \quad \forall v \in H^1(\Omega),\ A_i \in \mathcal{N}_h,$$

where the associated regular nodes set $\Lambda(A_i)$ and the coefficients $c(A_i)$ are defined in Lemma 3.2. Then for a given function $v \in H^1(\Omega)$, we define the interpolation $\Pi_{\mathcal{T}} v \in V_{\mathcal{T}}^1$ locally on each element $K \in \mathcal{T}$ as

$$\Pi_{\mathcal{T}} v|_K := \sum_{A_j \in \mathcal{N}_r(K)} N_j(v) \psi_j^K + \sum_{A_i \in \mathcal{N}_h(K)} \widetilde{N_i}(v) \psi_i^K. \tag{4.3}$$

Obviously, $\Pi_{\mathcal{T}} v \in V_{\mathcal{T}}^1 \subset V_{\mathcal{T}}^m$ for any positive integer $m$ and if $v|_{\partial\Omega} = 0$, then $\Pi_{\mathcal{T}} v|_{\partial\Omega} = 0$. Furthermore, the following local approximation properties hold (Theorem 9 in [19]).

**Lemma 4.1.** *For $K \in \mathcal{T}$, the operator $\Pi_{\mathcal{T}}$ defined in* (4.3) *satisfies*

$$|\Pi_{\mathcal{T}} v|_{1,K} \le C|v|_{1,\Omega_K} \qquad \forall v \in H^1(\Omega), \tag{4.4}$$

$$\|v - \Pi_{\mathcal{T}} v\|_{0,K} \le Ch_K |v|_{1,\Omega_K} \quad \forall v \in H^1(\Omega), \tag{4.5}$$

*where*

$$\Omega_K := \bigcup_{\widetilde{K} \in S(K)} \delta(\widetilde{K}) \quad \textit{with} \quad \delta(\widetilde{K}) := \bigcup_{K' \in S(\widetilde{K})} \overline{K'}$$

*and*

$$S(K) := \left\{ K_0 \in \mathcal{T} : \ \overline{K} \cap \overline{K_0} \neq \emptyset \right\}$$

*is the set of all the neighboring elements of the element $K \in \mathcal{T}$.*

**Corollary 4.1.** *For $E \in \mathcal{E}_0$, the operator $\Pi_{\mathcal{T}}$ defined in* (4.4) *satisfies*

$$\|v - \Pi_{\mathcal{T}} v\|_{0,E} \le Ch_E^{\frac{1}{2}} |v|_{1,\Omega_E} \quad \forall v \in H^1(\Omega), \tag{4.6}$$

*where $h_E := |E|^{\frac{1}{d-1}}$ and*

$$\Omega_E := \bigcup_{K_i \in \mathcal{T}, \overline{K_i} \cap E \in \mathcal{E}_0} \Omega_{K_i}.$$

*Proof.* If $E \in \mathcal{E}_s$, e.g., $\overline{A_0A_1}$ is shown as in Figure 4.1, then using scaled trace inequality we can obtain

$$\begin{aligned} \|v - \Pi_{\mathcal{T}} v\|_{0,E} &\le C \left( h_E^{-\frac{1}{2}} \|v - \Pi_{\mathcal{T}} v\|_{0,K_2} + h_E^{\frac{1}{2}} \|\nabla(v - \Pi_{\mathcal{T}} v)\|_{0,K_2} \right) \\ &\le Ch_E^{\frac{1}{2}} \|\nabla v\|_{0,\Omega_{K_2}} \le Ch_E^{\frac{1}{2}} |v|_{1,\Omega_E}. \end{aligned}$$

If $E \in \mathcal{E}_i$ (or $E \in \mathcal{E}_r$), e.g., $\overline{A_1A_2}$ (or $\overline{A_0A_7}$) shown in Figure 4.1, the proof will be similar to the above and $\Omega_E = \Omega_{K_1} \cup \Omega_{K_2} \cup \Omega_{K_3}$ (or $\Omega_E = \Omega_{K_2} \cup \Omega_{K_3}$). □

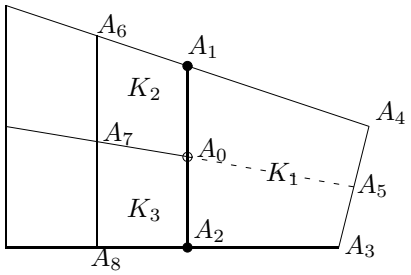


Fig. 4.1. An illustration of hanging node, irregular inner face and son-face.

Notice that the finite overlapping of patches $\Omega_K$ and $\Omega_E$ also holds on 1-irregular meshes. Next, we will present the residual-based a posteriori error estimate on 1-irregular meshes.

**Definition 4.1.** *For a mesh $\mathcal{T}_\ell$ and $v \in V_{\mathcal{T}_\ell}^m$, we define the element residual and jump residual for $v$ by*

$$R_K(v) := (f - \mathcal{L}v)|_K, \ \forall K \in \mathcal{T}_\ell \quad \text{and} \quad J(v)|_E := (\boldsymbol{A}\nabla v \cdot \nu_E)|_E, \ \forall E \in \mathcal{E}_0, \tag{4.7}$$

*where $[\![g]\!]$ is the jump of $g$ across an interior face $E$, and $\nu_E$ denotes a unit normal vector associated to face $E$. The error indicator for $v$ on $K \in \mathcal{T}_\ell$ is given by*

$$\eta_{\mathcal{T}_\ell}^2(v, K) = \eta_\ell^2(v, K) := h_K^2 \|R_K(v)\|_{L^2(K)}^2 + h_K \|J(v)\|_{L^2(\partial K \cap \Omega)}^2, \tag{4.8}$$

*where we recall $h_K = |K|^{\frac{1}{d}}$. For a subset $G \subset \mathcal{T}_\ell$ we set*

$$\eta_{\mathcal{T}_\ell}^2(v, G) = \eta_\ell^2(v, G) := \sum_{K \in G} \eta_{\mathcal{T}_\ell}^2(v, K). \tag{4.9}$$

If $u_\ell$ is the discrete solution of (4.2) and $G = \mathcal{T}_\ell$, let $\eta_\ell := \eta_{\mathcal{T}_\ell}(u_\ell, \mathcal{T}_\ell)$ for short. Hereafter, we denote $V_\ell = V_{\mathcal{T}_\ell}^m (V_h = V_{\mathcal{T}_h}^m)$ and set $e_h = u - u_h$, $e_H = u - u_H$ and $\varepsilon_H = u_h - u_H$ where $u$, $u_h$ and $u_H$ are the exact solution of (2.2), discrete solutions of (4.2) on $\mathcal{T}_h$ and $\mathcal{T}_H$ respectively. Notice "*Galerkin-orthogonality*" also holds for constrained finite element spaces defined on 1-irregular meshes, i.e.,

$$a(e_h, v_h) = 0 \quad \forall v_h \in V_h. \tag{4.10}$$

which illustrates $a(e_h, \varepsilon_H) = 0$ for $V_H \subset V_h$, but $a(\varepsilon_H, e_h) \neq 0$.

**Theorem 4.1.** *If the initial mesh-size $h_0$ is small enough, i.e., $h_0 < \min\{C_2, \hbar\}$ for a positive constant $C_2$, then there exists a positive constant $C_1$ with*

$$\|u - u_\ell\|_{a,\Omega}^2 \leq C_1 \eta_\ell^2. \tag{4.11}$$

The proof of Theorem 4.1 is similar to that for conforming triangular meshes [1, 2, 26]. The key ingredients are orthogonality (4.10), (4.5), (4.6) and Gårding's inequality (2.4). Here we omit the details.

Now we give the adaptive finite element algorithm as follows:

**Algorithm** AFEM

(0) Give the initial conforming quadrilateral or hexahedral mesh $\mathcal{T}_0$ and Döfler parameter $\theta \in (0, 1]$, and set $\ell = 0$;

(1) Solve (4.2) on $\mathcal{T}_\ell$ to get the solution $u_\ell$;

(2) Compute the error estimator $\eta_{\mathcal{T}_\ell}(u_\ell, K)$ for each element $K \in \mathcal{T}_\ell$;

(3) Mark the minimal elements set $\mathcal{M}_\ell$ such that

$$\eta_{\mathcal{T}_\ell}(u_\ell, \mathcal{M}_\ell) \geq \theta \eta_{\mathcal{T}_\ell}(u_\ell, \mathcal{T}_\ell); \tag{4.12}$$

(4) Refine $\mathcal{T}_\ell$ with $\mathcal{M}_\ell$ by Algorithm 3.1 to get $\mathcal{T}_{\ell+1}$;

(5) Set $\ell := \ell + 1$ and go to step (1).

The following theorem highlights the relationship between $e_h$ and $e_H$.

**Lemma 4.2 (Quasi-orthogonality)** *There exists a constant $C_5 > 0$ depending on the shape regularity and the data $\boldsymbol{A}$, $\boldsymbol{b}$ and $c$, and a number $s \in (0, 1]$ dictated only by the regularity of solution $u$ of (2.2), such that if the initial mesh-size $h_0$ satisfies $h_0^s \le \min\{C_5, \hbar^s\}$ then*

$$\|e_h\|_{a,\Omega}^2 \le \sigma \|e_H\|_{a,\Omega}^2 - \|\varepsilon_H\|_{a,\Omega}^2, \tag{4.13}$$

*where $\sigma \ge 1$ given in (4.17) at the last of proof can be made arbitrarily close to 1 by decreasing $h_0$.*

*Proof.* Expanding $a(e_H, e_H)$ and noticing $e_H = e_h + \varepsilon_H$ and (4.10) yield

$$a(e_h, e_h) = a(e_H, e_H) - a(\varepsilon_H, \varepsilon_H) - a(\varepsilon_H, e_h).$$

Using (4.10), Green's formula, Young's inequality with parameter $\delta > 0$ and (2.3) leads to

$$\begin{aligned} a(\varepsilon_H, e_h) =& a(e_h, \varepsilon_H) + (\mathbf{b} \cdot \nabla \varepsilon_H, e_h) - (\mathbf{b} \cdot \nabla e_h, \varepsilon_H) \\ =& 2(\mathbf{b} \cdot \nabla \varepsilon_H, e_h) + (\nabla \cdot \mathbf{b}\ e_h, \varepsilon_H) \\ \le& \Big( 2\|\mathbf{b}\|_{0,\infty,\Omega} \|\nabla \varepsilon_H\|_{0,\Omega} + \|\nabla \cdot \mathbf{b}\|_{0,\infty,\Omega} \|\varepsilon_H\|_{0,\Omega} \Big) \|e_h\|_{0,\Omega} \\ \le& C_b^2 \delta \|\varepsilon_H\|_{a,\Omega}^2 + \delta^{-1} \|e_h\|_{0,\Omega}^2, \end{aligned}$$

where the constant $C_b = \max\{2\|\mathbf{b}\|_{0,\infty,\Omega}, \|\nabla \cdot \mathbf{b}\|_{0,\infty,\Omega}\}/(2c_a)$. Furthermore, using Gårding's inequality (2.4) and (2.5) to estimate terms $a(e_h, e_h)$, $a(e_H, e_H)$ and $a(\varepsilon_H, \varepsilon_H)$ and combining with the above estimate, one can obtain

$$\begin{aligned} & \|e_h\|_{a,\Omega}^2 - (\gamma_G + \delta^{-1}) \|e_h\|_{0,\Omega}^2 \\ \le& \|e_H\|_{a,\Omega}^2 + \gamma_G \|e_H\|_{0,\Omega}^2 - (1 - C_b^2 \delta) \|\varepsilon_H\|_{a,\Omega}^2 + \gamma_G \|\varepsilon_H\|_{0,\Omega}^2. \end{aligned}$$

Taking the regularity $u \in H^{1+s}, s \in (0, 1]$ into account, and using the Aubin-Nitsche duality technique [13], one can easily show

$$\|e_h\|_{0,\Omega} \le C_3 h^s \|e_h\|_{1,\Omega}$$

where the constant $C_3$ depends only on the shape regularity and the data in (2.1). Hence

$$\|e_h\|_{0,\Omega} \le C_3 h_0^s \|e_h\|_{1,\Omega} \le \frac{C_3}{c_a} h_0^s \|e_h\|_{a,\Omega}.$$

Similarly, we have

$$\|e_H\|_{0,\Omega} \le \frac{C_3}{c_a} h_0^s \|e_H\|_{a,\Omega}.$$

Noticing

$$\|\varepsilon_H\|_{0,\Omega}^2 \le 2\|e_h\|_{0,\Omega}^2 + 2\|e_H\|_{0,\Omega}^2$$

and setting $C_4 := C_3/c_a$ lead to

$$\begin{aligned} & \Big( 1 - C_4^2 (3\gamma_G + \delta^{-1}) h_0^{2s} \Big) \|e_h\|_{a,\Omega} \\ \le& \Big( 1 + 3\gamma_G C_4^2 h_0^{2s} \Big) \|e_H\|_{a,\Omega} - \Big( 1 - C_b^2 \delta \Big) \|\varepsilon_H\|_{a,\Omega}. \end{aligned} \tag{4.14}$$

Let $1 - C_4^2(3\gamma_G + \delta^{-1})h_0^{2s} = 1 - C_b^2\delta$. We have

$$\delta = \frac{3\gamma_G C_4^2 h_0^{2s} + \sqrt{9\gamma_G^2 C_4^4 h_0^{4s} + 4C_b^2 C_4^2 h_0^{2s}}}{2C_b^2} > 0.$$

We should further choose $h_0$ sufficiently small so that $1 - C_b^2\delta > 0$. Notice that

$$\delta < \frac{3\gamma_G C_4^2 h_0^{2s} + 3\gamma_G C_4^2 h_0^{2s} + 2C_b C_4 h_0^s}{2C_b^2}, \tag{4.15}$$

and if

$$\frac{3\gamma_G C_4^2 h_0^{2s} + 3\gamma_G C_4^2 h_0^{2s} + 2C_b C_4 h_0^s}{2C_b^2} \le \frac{1}{C_b^2} \tag{4.16}$$

holds, then $1 - C_b^2\delta > 0$ must hold, i.e., we only require $h_0^s \le C_5$, where the constant

$$C_5 = \frac{-C_b C_4 + \sqrt{C_b^2 C_4^2 + 12\gamma_G C_4^4}}{6\gamma_G C_4^2} > 0$$

is the positive root of (4.16). Multiplying two sides of (4.14) by $1/(1 - C_b^2\delta)$ and using (4.15) yield

$$\|e_h\|_{a,\Omega}^2 \le \sigma \|e_H\|_{a,\Omega}^2 - \|\varepsilon_H\|_{a,\Omega}^2 \quad \text{with } \sigma = \frac{1 + 3\gamma_G C_4^2 h_0^{2s}}{1 - 3\gamma_G C_4^2 h_0^{2s} - C_b C_4 h_0^s}. \tag{4.17}$$

This completes the proof of lemma. □

**Remark 4.1.** If $\mathbf{b} = 0$, then the following orthogonality holds without any restriction on $h_0$:

$$\|e_h\|_{a,\Omega}^2 = \|e_H\|_{a,\Omega}^2 - \|\varepsilon_H\|_{a,\Omega}^2. \tag{4.18}$$

**Lemma 4.3.** *Let $\mathcal{T}_\ell$ be a shape regular mesh. Then there exists a constant $C$ depending only on the shape regularity and polynomials degree $m$, such that for any $v \in V_\ell$ the following inequality holds:*

$$\|D^2 v\|_{0,K} \le C h_K^{-1} \|\nabla v\|_{0,K} \quad \forall K \in \mathcal{T}_\ell, \tag{4.19}$$

*where $D^2 v$ is the Hessian of $v$.*

*Proof.* We only prove the inequality in 2D-case and the 3D-case is similar. Since

$$\frac{\partial v}{\partial x} = \frac{\partial \hat{v}}{\partial \hat{x}} \cdot \frac{\partial \hat{x}}{\partial x} + \frac{\partial \hat{v}}{\partial \hat{y}} \cdot \frac{\partial \hat{y}}{\partial x}$$

and

$$\frac{\partial^2 v}{\partial x^2} = \frac{\partial^2 \hat{v}}{\partial \hat{x}^2}\left(\frac{\partial \hat{x}}{\partial x}\right)^2 + \frac{\partial^2 \hat{v}}{\partial \hat{y}^2}\left(\frac{\partial \hat{y}}{\partial x}\right)^2 + 2\frac{\partial^2 \hat{v}}{\partial \hat{x}\partial \hat{y}}\frac{\partial \hat{y}}{\partial x}\frac{\partial \hat{x}}{\partial x} + \frac{\partial \hat{v}}{\partial \hat{x}}\frac{\partial^2 \hat{x}}{\partial x^2} + \frac{\partial \hat{v}}{\partial \hat{y}}\frac{\partial^2 \hat{y}}{\partial x^2},$$

we obtain

$$\begin{aligned}\|v_{xx}\|_{0,K} \le & C|K|^{\frac{1}{2}}\Big((\|\hat{v}_{\hat{x}\hat{y}}\|_{0,\hat{K}} + \|\hat{v}_{\hat{x}\hat{x}}\|_{0,\hat{K}} + \|\hat{v}_{\hat{y}\hat{y}}\|_{0,\hat{K}})\|DF_K^{-1}\|^2 \\ & + \|\hat{\nabla}\hat{v}\|_{0,\hat{K}}\|D^2 F_K^{-1}\|\Big).\end{aligned}$$

Notice that

$$\|\hat{v}_{\hat{x}\hat{y}}\|_{0,\hat{K}} + \|\hat{v}_{\hat{x}\hat{x}}\|_{0,\hat{K}} + \|\hat{v}_{\hat{y}\hat{y}}\|_{0,\hat{K}} \leq C|\hat{\nabla}\hat{v}|_{1,\hat{K}} \leq C\|\hat{\nabla}\hat{v}\|_{1,\hat{K}} \leq C\|\hat{\nabla}\hat{v}\|_{0,\hat{K}},$$

where the last inequality is due to the equivalence of norms of finite dimension space (polynomials space $(\mathbb{Q}_m(\hat{K}))^d$) over reference element $\hat{K}$. Furthermore, since $\mathcal{T}_\ell$ is shape regular, we have

$$\|DF_K^{-1}\| \leq Ch_K^{-1}, \quad \text{and} \quad \|D^2F_K^{-1}\| \leq \|D^2F_K\| \cdot \|DF_K^{-1}\|^3 \leq Ch_K^{-1}.$$

Therefore, we arrive at

$$\|v_{xx}\|_{0,K} \leq C|K|^{\frac{1}{2}}(h_K^{-2} + h_K^{-1})\|\hat{\nabla}\hat{v}\|_{0,\hat{K}} \leq Ch_K^{-1}\|\hat{\nabla}\hat{v}\|_{0,\hat{K}} \leq Ch_K^{-1}\|\nabla v\|_{0,K}.$$

We can estimate other terms in $D^2v$ in the same way. □

**Lemma 4.4.** *Let $\mathcal{T}_\ell$ be a shape regular mesh. For all $K \in \mathcal{T}_\ell$ and any $v, w \in V_\ell$, we have*

$$\eta_\ell(v, K) \leq \eta_\ell(w, K) + C\|v - w\|_{1,\omega_K}, \tag{4.20}$$

*where*

$$\omega_K := \bigcup_{\substack{\overline{K_i} \cap E \in \mathcal{E}_0 \\ K_i \in \mathcal{T}_\ell, E \in \mathcal{E}(K)}} K_i$$

*and $C > 0$ is a constant depending only on the shape regularity, the polynomial degree $m$ and the coefficients $\boldsymbol{A}$, $\boldsymbol{b}$ and $c$ in elliptic operator $\mathcal{L}$.*

*Proof.* By adding and subtracting $w$ and using triangle inequality, we obtain

$$\eta_\ell(v, K) \leq \eta_\ell(w, K) + h_K\|\mathcal{L}(v - w)\|_{L^2(K)} + h_K^{\frac{1}{2}}\|J(v - w)\|_{L^2(\partial K \cap \Omega)}.$$

Using

$$\mathcal{L}(v - w) = \mathrm{div}\mathbf{A}\nabla(v - w) - \mathbf{b} \cdot \nabla(v - w) - c(v - w),$$

we have

$$\|\mathcal{L}(v - w)\|_{L^2(K)} \leq \|\mathrm{div}\mathbf{A}\nabla(v - w)\|_{L^2(K)} + \|\mathbf{b} \cdot \nabla(v - w)\|_{L^2(K)} + \|c(v - w)\|_{L^2(K)}.$$

Notice that

$$\mathrm{div}\mathbf{A}\nabla(v - w) = \mathrm{div}\mathbf{A} \cdot \nabla(v - w) + \mathbf{A} : D^2(v - w),$$

where $D^2(v - w)$ is the Hessian of $v - w$. Using Lemma 4.3, we can derive

$$\begin{aligned}\|\mathcal{L}(v - w)\|_{L^2(K)} \leq & \|\mathrm{div}\mathbf{A}\|_{0,\infty,\Omega}\|\nabla(v - w)\|_{0,K} + h_K^{-1}\|\mathbf{A}\|_{0,\infty,\Omega}\|\nabla(v - w)\|_{0,K} \\ & + \|\mathbf{b}\|_{0,\infty,\Omega}\|\nabla(v - w)\|_{0,K} + \|c\|_{0,\infty,\Omega}\|v - w\|_{0,K}.\end{aligned}$$

We now deal with the jump residual. Let $E$ be a face of $K$. For convenience, let $K$ be the element $K_2$ and $E$ be the edge $\overline{A_1A_0}$ shown in Figure 4.1. Denote $K'$ to be the quadrilateral $\overline{A_0A_1A_4A_5}$ where node $A_5$ is the midpoint of edge $\overline{A_4A_3}$. Then

$$J(v - w)|_E = ((\mathbf{A}\nabla(v - w))|_K - (\mathbf{A}\nabla(v - w))|_{K'}) \cdot \nu_E.$$

By scaled trace inequality and Lemma 4.3, we can obtain

$$\|(\mathbf{A}\nabla(v-w))|_K \cdot \nu_E\|_{0,E} \leq Ch_K^{-\frac{1}{2}}\|\mathbf{A}\|_{0,\infty,\Omega}\|\nabla(v-w)\|_{0,K}.$$

The same argument holds for $K'$ and since $\mathcal{T}_\ell$ is shape regular, we can replace $h_{K'}$ by $h_K$. If $K$ is the element $K_1$ and $E$ is the edge $\overline{A_1A_2}$ shown in Figure 4.1, then we can choose $K'$ to be the quadrilateral $\overline{A_1A_2A_8A_6}$ and prove the result similarly. Furthermore, we can also estimate jump residual in 3D-case similarly. Finally, collecting the above estimates for $K$ and all its neighbors yields (4.20). □

**Lemma 4.5.** *For a 1-irregular mesh $\mathcal{T}_\ell$ and a subset $\mathcal{M}_\ell \subset \mathcal{T}_\ell$, let $\mathcal{T}_{\ell+1} = REFINE(\mathcal{T}_\ell, \mathcal{M}_\ell)$. Then there exist constants $\lambda := 1 - \chi^{\frac{1}{d}} \in (0,1)$ and $C_2 > 0$ depending only on the shape regularity, the polynomial degree $m$ and the coefficients $\boldsymbol{A}$, $\boldsymbol{b}$ and $c$ in elliptic operator $\mathcal{L}$, such that for any $\delta > 0$, any $v_\ell \in V_\ell$ and any $v_{\ell+1} \in V_{\ell+1}$*

$$\begin{aligned}\eta_{\ell+1}^2(v_{\ell+1},\mathcal{T}_{\ell+1}) \leq &(1+\delta)\eta_\ell^2(v_\ell,\mathcal{T}_\ell) - \lambda(1+\delta)\eta_\ell^2(v_\ell,\mathcal{M}_\ell)\\ &+ C_2(1+1/\delta)\|v_{\ell+1}-v_\ell\|_{a,\Omega}^2. \end{aligned} \tag{4.21}$$

*Proof.* Applying Lemma 4.4 with $v_\ell \in V_\ell$, $v_{\ell+1} \in V_{\ell+1}$ over $K \in \mathcal{T}_{\ell+1}$, using Young's inequality with parameter $\delta$ and the summation over all elements $K \in \mathcal{T}_{\ell+1}$ together with the finite overlap property of patches $\omega_K$ and the equivalence of the $H^1$ norm and the energy norm in $\Omega$, one can get

$$\eta_{\ell+1}^2(v_{\ell+1},\mathcal{T}_{\ell+1}) \leq (1+\delta)\eta_{\ell+1}^2(v_\ell,\mathcal{T}_{\ell+1}) + C_2(1+1/\delta)\|v_{\ell+1}-v_\ell\|_{a,\Omega}^2 .$$

For a marked element $K \in \mathcal{M}_\ell \subset \mathcal{T}_\ell$, we set $\mathcal{T}_{\ell+1,K} := \{K' \in \mathcal{T}_{\ell+1} \mid K' \subset K\}$. Since $v_\ell \in V_\ell \subset V_{\ell+1}$, we see that $J(v_\ell) = 0$ on sides of $\mathcal{T}_{\ell+1,K}$ in the interior of $K$. By Lemma 3.1, we obtain

$$h_{K'} = |K'|^{\frac{1}{d}} \leq \chi^{\frac{1}{d}} h_K$$

which yields

$$\eta_{\ell+1}^2(v_\ell,K) = \sum_{K'\in\mathcal{T}_{\ell+1,K}} \eta_{\ell+1}^2(v_\ell,K') \leq \chi^{\frac{1}{d}}\eta_\ell^2(v_\ell,K).$$

For an element $K \in \mathcal{T}_{\ell+1}\backslash\mathcal{M}_\ell$, one can also obtain $\eta_{\ell+1}(v_{\ell+1},K) \leq \eta_\ell(v_{\ell+1},K)$. Hence, summing over all $K \in \mathcal{T}_{\ell+1}$, we obtain

$$\begin{aligned}\eta_{\ell+1}^2(v_\ell,\mathcal{T}_{\ell+1}) =&\eta_{\ell+1}^2(v_\ell,\mathcal{T}_{\ell+1}\backslash\mathcal{M}_\ell) + \eta_{\ell+1}^2(v_\ell,\mathcal{M}_\ell)\\ \leq&\eta_\ell^2(v_\ell,\mathcal{T}_\ell\backslash\mathcal{M}_\ell) + \chi^{\frac{1}{d}}\eta_\ell^2(v_\ell,\mathcal{M}_\ell)\\ \leq&\eta_\ell^2(v_\ell,\mathcal{T}_\ell) - (1-\chi^{\frac{1}{d}})\eta_\ell^2(v_\ell,\mathcal{M}_\ell) .\end{aligned}$$

Setting $\lambda = 1 - \chi^{\frac{1}{d}} \in (0,1)$ leads to the final result. □

Set $e_{\ell+1} = u - u_{\ell+1}$, $e_\ell = u - u_\ell$ and $\varepsilon_\ell = u_{\ell+1} - u_\ell$. Then we have the following convergence result.

**Theorem 4.2 (Energy Reduction)** *Let $\{\mathcal{T}_\ell, u_\ell\}_{\ell\geq 0}$ be the sequence of meshes and discrete solutions produced by $\mathcal{AFEM}$ . Then there exist constants $\beta > 0$ and $0 < \alpha < 1$ depending*

*on the shape regularity of $\mathcal{T}_0$, the marking parameter $0 < \theta \leq 1$, the polynomial degree $m$ and the coefficients $\boldsymbol{A}$, $\boldsymbol{b}$ and $c$ in elliptic operator $\mathcal{L}$, such that if the initial mesh-size $h_0$ is small enough, we have*

$$\|e_{\ell+1}\|_{a,\Omega}^2 + \beta\eta_{\ell+1}^2 \leq \alpha\Big(\|e_\ell\|_{a,\Omega}^2 + \beta\eta_\ell^2\Big). \tag{4.22}$$

*Proof.* For $t \in (0,1)$, using quasi-orthogonality (4.13), Lemma 4.5 and Theorem 4.1, we have

$$\begin{aligned}
&\|e_{\ell+1}\|_{a,\Omega}^2 + \beta\eta_{\ell+1}^2\\
\leq&\sigma\|e_\ell\|_{a,\Omega}^2 - \|\varepsilon_\ell\|_{a,\Omega}^2 + \beta\eta_{\ell+1}^2\\
\leq&\sigma\|e_\ell\|_{a,\Omega}^2 - \|\varepsilon_\ell\|_{a,\Omega}^2 + \beta\Big((1+\delta)\eta_\ell^2 - \lambda(1+\delta)\eta_\ell^2(\mathcal{M}_\ell) + C_2(1+1/\delta)\|\varepsilon_\ell\|_{a,\Omega}^2\Big)\\
\leq&\sigma\|e_\ell\|_{a,\Omega}^2 - \|\varepsilon_\ell\|_{a,\Omega}^2 + \beta\Big((1+\delta)\eta_\ell^2 - \lambda\theta(1-t+t)(1+\delta)\eta_\ell^2 + \ C_2(1+1/\delta)\|\varepsilon_\ell\|_{a,\Omega}^2\Big)\\
=&\sigma\|e_\ell\|_{a,\Omega}^2 - \|\varepsilon_\ell\|_{a,\Omega}^2 + \beta(1+\delta)\big(1-\lambda\theta(1-t)\big)\eta_\ell^2 - \ \beta\lambda\theta t(1+\delta)\eta_\ell^2 + \ C_2\beta(1+1/\delta)\|\varepsilon_\ell\|_{a,\Omega}^2\\
\leq&\big(\sigma - \frac{\beta\lambda\theta t(1+\delta)}{C_1}\big)\|e_\ell\|_{a,\Omega}^2 + \beta(1+\delta)\big(1-\lambda\theta(1-t)\big)\eta_\ell^2 + \ \big(C_2\beta(1+1/\delta)-1\big)\|\varepsilon_\ell\|_{a,\Omega}^2.
\end{aligned}$$

Now we need to choose appropriate values for each parameter to satisfy the following three conditions.

(i) $(1+\delta)\big(1-\lambda\theta(1-t)\big) < 1$; This condition is equivalent to $t < 1 - \delta/\lambda\theta(1+\delta)$. Since $t \in (0,1)$, we need to restrict $\delta$ small enough to satisfy

$$1 - \frac{\delta}{\lambda\theta(1+\delta)} > 0.$$

(ii) $C_2\beta(1+1/\delta) - 1 \leq 0$; to satisfy this condition we should restrict

$$0 < \beta < \frac{1}{C_2(1+1/\delta)}.$$

(iii) $\sigma - \beta\lambda\theta t(1+\delta)/C_1 < 1$; by setting $C_7 := \beta\lambda\theta t(1+\delta)/C_1$ and noticing (4.17) we have

$$\sigma = \frac{1 + 3\gamma_G C_4^2 h_0^{2s}}{1 - 3\gamma_G C_4^2 h_0^{2s} - C_b C_4 h_0^s} < 1 + C_7,$$

which implies

$$h_0^s < \frac{-(C_7+1)C_bC_4 + \sqrt{(C_7+1)^2C_b^2C_4^2 + 12(2\gamma_G + C_7)C_4^2C_7}}{6(2\gamma_G + C_7)C_4^2}.$$

Denote by $C_6 :=$ the right-hand side above (which is positive). Then we know choosing $\delta$ small enough and taking $h_0^s < \min\{C_6, C_5, C_2^s, \hbar^s\}$ can yield

$$\alpha := \max\left\{\sigma - \frac{\beta\lambda\theta t(1+\delta)}{C_1}, (1+\delta)\big(1-\lambda\theta(1-t)\big)\right\} < 1,$$

which is the desired result. □

**Remark 4.2.** If $\mathbf{b} = 0$, then using the orthogonality (4.18), we can obtain the same convergence result similarly without assuming that the initial meshsize $h_0$ is small enough.

## 5. Implementation on 1-irregular Meshes

As we know, for constrained finite element spaces on meshes with hanging nodes, if one uses the original basis functions to assemble stiff matrix, then the resulting linear system will like a "saddle system". Hence it is not advisable to do this. In this section, we will first discuss explicitly how to obtain a symmetric positive definite linear algebraic system, which is useful for implementation. Define the discontinuous finite element spaces without any constraints on 1-irregular mesh $\mathcal{T}$ as:

$$\mathbb{D}_{\mathcal{T}}^m := \left\{ v \in L^2(\Omega) \mid v_{|_K} \circ F_K \in \mathbb{Q}_m(\hat{K}),\ \forall K \in \mathcal{T} \right\}, \tag{5.1}$$

where the degrees of freedom are taken with the usual Lagrange or Serendipity conforming finite element spaces. Furthermore, we give the constrained finite element spaces with nonhomogeneous boundary as:

$$\mathbb{V}_{\mathcal{T}}^m := \mathbb{D}_{\mathcal{T}}^m \cap H^1(\Omega). \tag{5.2}$$

For an element $K \in \mathcal{T}$, a finite element function $u \in \mathbb{D}_{\mathcal{T}}^m$ restricted on $K$ can be written as $u|_K := \sum_{i=0}^s u_i^K \psi_i^K$ where $U^K := \{u_0^K, u_1^K, \cdots, u_s^K\}$ is the set of all the nodal variables(or degrees of freedom) of $K$ and $\psi^K := \{\psi_0^K, \psi_1^K, \cdots, \psi_s^K\}$ is the set of all the usual local mapped basis functions restricted on element $K$ with respect to the degree of freedom $u_i^K$, i.e., $\psi_i^K \circ F_K \in \mathbb{Q}_m(\hat{K})$. We also denote by $A^K := \{A_0^K, A_1^K, \cdots, A_s^K\}$ the set of the nodes with respect to $\psi^K$ which means $\psi_j^K(A_i^K) = \delta_{ij}$. In addition, let $n := dim(\mathbb{D}_{\mathcal{T}}^m)$ be the the number of all degrees of freedom on the whole mesh $\mathcal{T}$ and denote by $U := \{u_1, u_2, \cdots, u_n\}$ the set of all the degrees of freedom, $\psi := \{\psi_1, \psi_2, \cdots, \psi_n\}$ the set of all the basis functions and $\mathcal{A} := \{A_1, A_2, \cdots, A_n\}$ the set of all the nodes with respect to $\psi$. Obviously,

$$U^K \subset U, A^K \subset \mathcal{A} \quad \text{and} \quad \psi_i = \sum_{K \in \mathcal{T}, A_j^K = A_i} \psi_j^K$$

for any basis function $\psi_i \in \psi$. By the way, if $m = 1$, then $\mathcal{A} = \mathcal{N}$ based on the definition of $\mathcal{N}$ in the last section. As we know, a piecewise infinitely differentiable function $u$ in $\mathbb{D}_{\mathcal{T}}^m$ belongs to $H^1(\Omega)$ if and only if $u$ is continuous across any inter-element $(d-1)$-dimensional face which in fact implies the constraints on finite element spaces $\mathbb{V}_{\mathcal{T}}^m$. Obviously, any function $u \in \mathbb{D}_{\mathcal{T}}^m$ is continuous across any regular face $E \in \mathcal{E}_r$, i.e., constraints are only required on any irregular face $E \in \mathcal{E}_i$. Take Figure 3.2 as an example, where $A$ is a hanging node, $E \in \mathcal{E}_i$ and $E_1, E_2 \in \mathcal{E}_s$. Let $u_0^K, u_1^K, \cdots, u_m^K \in U^K$ be the nodal variables (or degrees of freedom) of $K$ located on edge $E$. Similarly, let $u_0^{K_1}, u_1^{K_1}, \cdots, u_m^{K_1} \in U^{K_1}$ be the nodal variables of $K_1$ located on edge $E_1$ and $u_0^{K_2}, u_1^{K_2}, \cdots, u_m^{K_2} \in U^{K_2}$ be the nodal variables of $K_2$ located on edge $E_2$. So are the other quantities like basis function in $\psi$ and node in $\mathcal{A}$. In order to keep the continuity across $E$, the following constraints should be satisfied:

$$u_i^{K_1} = \sum_{j=0}^m u_j^K \psi_j^K(A_i^{K_1}), \quad i = 0, 1, \cdots, m; \tag{5.3}$$

$$u_i^{K_2} = \sum_{j=0}^m u_j^K \psi_j^K(A_i^{K_2}), \quad i = 0, 1, \cdots, m. \tag{5.4}$$

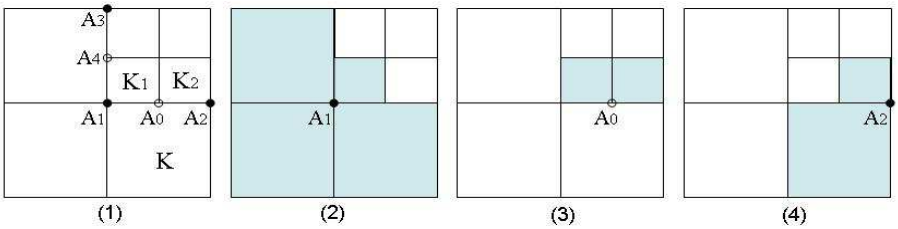


Fig. 5.1. $A_1$ and $A_2$ are regular nodes with respect to two unconstrained nodal variables $u_1$ and $u_2$; $A_0$ is a hanging node with respect to a constrained nodal variable $u_0$; Green areas in (2),(3) and (4) are to show $supp(\psi_1)$, $supp(\psi_0)$ and $supp(\psi_2)$ respectively.

### 5.1. $Q_1$ element in 2D-case.

In order to keep the continuity on edge $\overline{A_1A_2}$ shown in Figure 5.1, constraints (5.3) and (5.4) should be satisfied which can be simplified as:

$$u_0 = \frac{u_1 + u_2}{2}. \tag{5.5}$$

Constrain (5.5) tells us $u_1$ and $u_2$ are really effective degrees of freedom while $u_0$ is not. Moreover, if we drop the degree of freedom $u_0$ and modify the basis functions $\psi_1$ and $\psi_2$ as follows:

$$\widetilde{\psi_1} = \psi_1 + \frac{1}{2}\psi_0, \quad \widetilde{\psi_2} = \psi_2 + \frac{1}{2}\psi_0, \tag{5.6}$$

then the continuity on edge $\overline{A_1A_2}$ will be satisfied automatically. So is the edge $\overline{A_1A_3}$. Similarly, we can obtain explicit formulas of constraints for higher order and higher dimensional finite element spaces as illustrated by Figure 5.2.

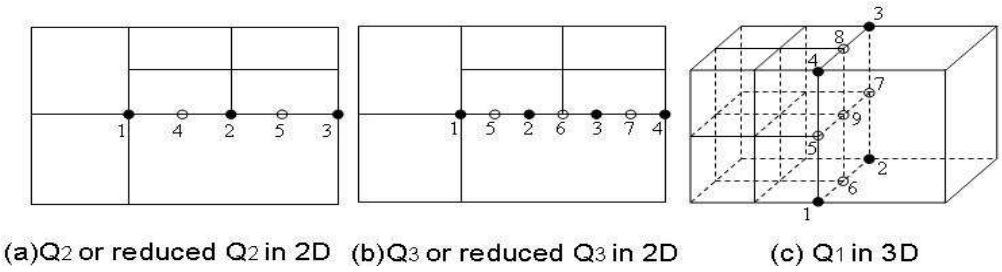


Fig. 5.2. Index $i$ corresponds to a node $A_i$, a nodal variable $u_i$ and a basis function $\psi_i$; Solid balls stand for the unconstrained nodal variables while hollow balls stand for the constrained nodal variables.

### 5.2. $Q_2$ or reduced $Q_2$ element in 2D-case.

In order to keep the continuity on edge $\overline{A_1A_3}$ shown in Figure 5.2-(a), we let:

$$u_4 = \frac{3}{8}u_1 + \frac{3}{4}u_2 - \frac{1}{8}u_3, \tag{5.7a}$$

$$u_5 = -\frac{1}{8}u_1 + \frac{3}{4}u_2 + \frac{3}{8}u_3. \tag{5.7b}$$

Although vertex $A_2$ shown in Figure 5.2-(a) is a hanging node, the corresponding degree of freedom $u_2$ is an unconstrained nodal variable in this case. We can also drop $u_4$ and $u_5$ and

modify the basis functions to ensure the continuity on edge $\overline{A_1A_3}$ automatically, i.e.,

$$\widetilde{\psi_1} = \psi_1 + \frac{3}{8}\psi_4 - \frac{1}{8}\psi_5, \tag{5.8a}$$

$$\widetilde{\psi_2} = \psi_2 + \frac{3}{4}\psi_4 + \frac{3}{4}\psi_5, \tag{5.8b}$$

$$\widetilde{\psi_3} = \psi_3 - \frac{1}{8}\psi_4 + \frac{3}{8}\psi_5. \tag{5.8c}$$

### 5.3. $Q_3$ or reduced $Q_3$ element in 2D-case.

In order to keep the continuity on edge $\overline{A_1A_4}$ shown in Figure 5.2-(b), we let:

$$u_5 = \frac{5}{16}u_1 + \frac{15}{16}u_2 - \frac{5}{16}u_3 + \frac{1}{16}u_4, \tag{5.9a}$$

$$u_6 = -\frac{1}{8}u_1 + \frac{9}{16}u_2 + \frac{9}{16}u_3 - \frac{1}{8}u_4, \tag{5.9b}$$

$$u_7 = \frac{1}{16}u_1 - \frac{5}{16}u_2 + \frac{15}{16}u_3 + \frac{5}{16}u_4. \tag{5.9c}$$

Notice $u_2$ and $u_3$ are two unconstrained nodal variables in this case. We can also drop $u_5$, $u_6$ and $u_7$ and modify the basis functions to ensure the continuity on edge $\overline{A_1A_4}$ automatically, i.e.,

$$\widetilde{\psi_1} = \psi_1 + \frac{5}{16}\psi_5 - \frac{1}{8}\psi_6 + \frac{1}{16}\psi_7, \tag{5.10a}$$

$$\widetilde{\psi_2} = \psi_2 + \frac{15}{16}\psi_5 + \frac{9}{16}\psi_6 - \frac{5}{16}\psi_7, \tag{5.10b}$$

$$\widetilde{\psi_3} = \psi_3 - \frac{5}{16}\psi_5 + \frac{9}{16}\psi_6 + \frac{15}{16}\psi_7, \tag{5.10c}$$

$$\widetilde{\psi_4} = \psi_4 + \frac{1}{16}\psi_5 - \frac{1}{8}\psi_6 + \frac{5}{16}\psi_7. \tag{5.10d}$$

### 5.4. $Q_1$ element in 3D-case.

In order to keep the continuity on face $\overline{A_1A_2A_3A_4}$ shown in Figure 5.2-(c), we let:

$$u_5 = \frac{u_4 + u_1}{2}, \quad u_6 = \frac{u_1 + u_2}{2}, \tag{5.11a}$$

$$u_7 = \frac{u_2 + u_3}{2}, \quad u_8 = \frac{u_3 + u_4}{2}, \tag{5.11b}$$

$$u_9 = \frac{u_1 + u_2 + u_3 + u_4}{4}. \tag{5.11c}$$

We can also drop $u_5$, $u_6$, $u_7$, $u_8$ and $u_9$ and modify the basis functions to ensure the continuity on face $\overline{A_1A_2A_3A_4}$ automatically, i.e.,

$$\widetilde{\psi_1} = \psi_1 + \frac{1}{2}\psi_5 + \frac{1}{2}\psi_6 + \frac{1}{4}\psi_9, \tag{5.12a}$$

$$\widetilde{\psi_2} = \psi_2 + \frac{1}{2}\psi_6 + \frac{1}{2}\psi_7 + \frac{1}{4}\psi_9, \tag{5.12b}$$

$$\widetilde{\psi_3} = \psi_3 + \frac{1}{2}\psi_7 + \frac{1}{2}\psi_8 + \frac{1}{4}\psi_9, \tag{5.12c}$$

$$\widetilde{\psi_4} = \psi_4 + \frac{1}{2}\psi_5 + \frac{1}{2}\psi_8 + \frac{1}{4}\psi_9. \tag{5.12d}$$

Let us discuss the unified formulas of the above modified bases for constrained finite element space $\mathbb{V}_{\mathcal{T}}^m$. For a basis function $\psi_j$ and its corresponding node $A_j$, if there exists another basis function $\psi_i$ such that $\psi_i(A_j) \neq 0$, then the degree of freedom $u_j$ with respect to $\psi_j$ must be constrained by the degree of freedom $u_i$ with respect to $\psi_i$. We use the index set $I_c$ to indicate all the actually constrained degrees of freedom, i.e., if $i \in I_c$, then $u_i$ is a constrained degree of freedom. Similarly, we use $I_r$ to indicate all the actually unconstrained degrees of freedom ($I_c \cup I_r = \{1, \cdots, n\}$). Then the above modified (constrain-free) basis can be written as

$$\widetilde{\psi}_i = \psi_i + \sum_{j \in I_c, \psi_i(A_j) \neq 0} \psi_i(A_j)\psi_j \quad \forall i \in I_r. \tag{5.13}$$

Denote by $u_1, u_2, \cdots, u_r$ all the actually unconstrained degrees of freedom and $\widetilde{\psi_1}, \cdots, \widetilde{\psi_r}$ all the corresponding modified basis functions. Then any function $u = \sum_{i=1}^n u_i\psi_i \in \mathbb{V}_{\mathcal{T}}^m$ can be written as:

$$u = \sum_{i=1}^{r} u_i\widetilde{\psi}_i. \tag{5.14}$$

Notice any function with the formula (5.14) must belong to $\mathcal{C}^0(\overline{\Omega})$. More importantly, using the above modified basis functions to assemble stiff matrix will yield a symmetric positive definite linear system. In fact, the technique herein to expand the compactly supported set of some original basis functions is in some sense, like the well-known "macro-element" (Hsieh-Clough-Tocher element) technique [14].

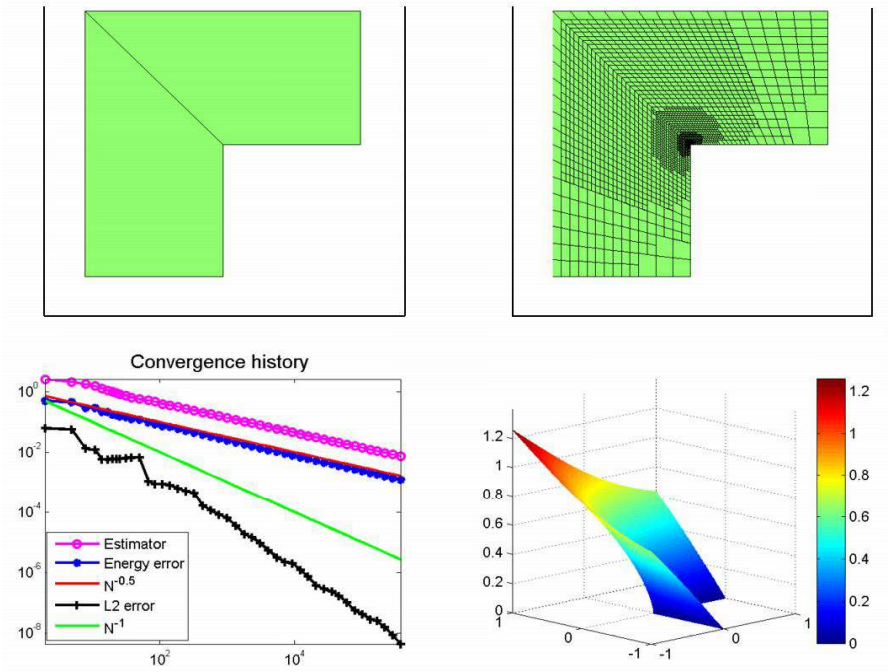


Fig. 5.3. (Top left) Initial mesh; (Bottom left) Convergence history of algorithm $\mathcal{AFEM}$ for L-shaped domain problem with Döfler parameter $\theta = 0.3$; (Top right) A medial adaptive mesh of level 25 with 1808 elements; (Bottom right) The surface plot of finite element solution on the final mesh with 372116 elements.

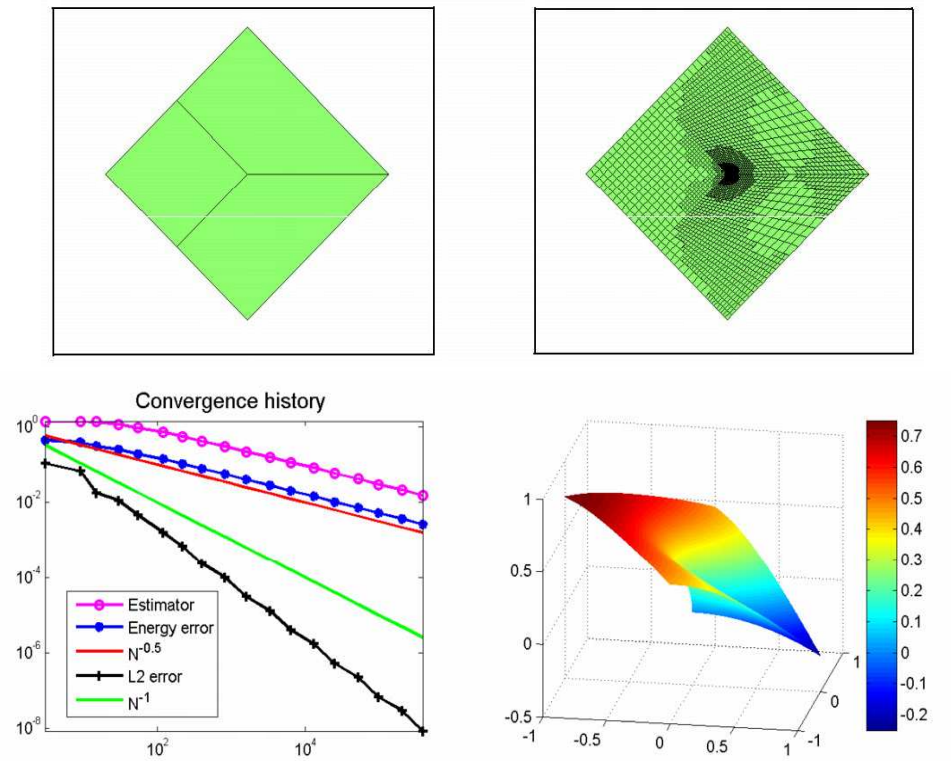


Fig. 5.4. (Top left) Initial mesh; (Bottom left) Convergence history of algorithm $\mathcal{AFEM}$ for Crack problem with Döfler parameter $\theta = 0.8$; (Bottom right) A medial adaptive mesh of level 10 with 1599 elements; (Top right) The surface plot of finite element solution on the final mesh with 393297 elements.

Now we give several numerical experiments with quadrialteral $\mathbb{Q}_1$ element.

**Example 5.1.** (***L-shaped domain***) *The first experiment is to solve the Laplace equation* $-\Delta u = 0$ *with Dirichlet boundary condition in the L-shaped domain* $\Omega = (-1,1) \times (0,1) \cup (-1,0) \times (-1,0]$, *where the exact solution is given in polar coordinates by*

$$u(r,\theta) = r^{\frac{2}{3}} \sin(2\theta/3).$$

We compute the posteriori error estimator, energy error and the $L^2$ error on each mesh, respectively. Figure 5.3 evidently shows our adaptive algorithm is optimally convergent.

**Example 5.2.** (***Crack problem***) *Let* $\Omega = \{|x| + |y| < 1\} \backslash \{0 \le x \le 1, y = 0\}$ *with a crack and assume that the solution* $u$ *satisfies the Poisson equation*

$$-\triangle u = 1, \ \textit{in } \Omega \quad \textit{and} \quad u = g \ \textit{on } \partial\Omega.$$

*We choose* $g$ *such that the exact solution* $u$ *in polar coordinates is*

$$u(r,\theta) = r^{\frac{1}{2}} \sin\frac{\theta}{2} - \frac{1}{4} r^2.$$

From Figure 5.4, one can see the advantage of algorithm $\mathcal{AFEM}$ for the Crack problem which is optimally convergent.

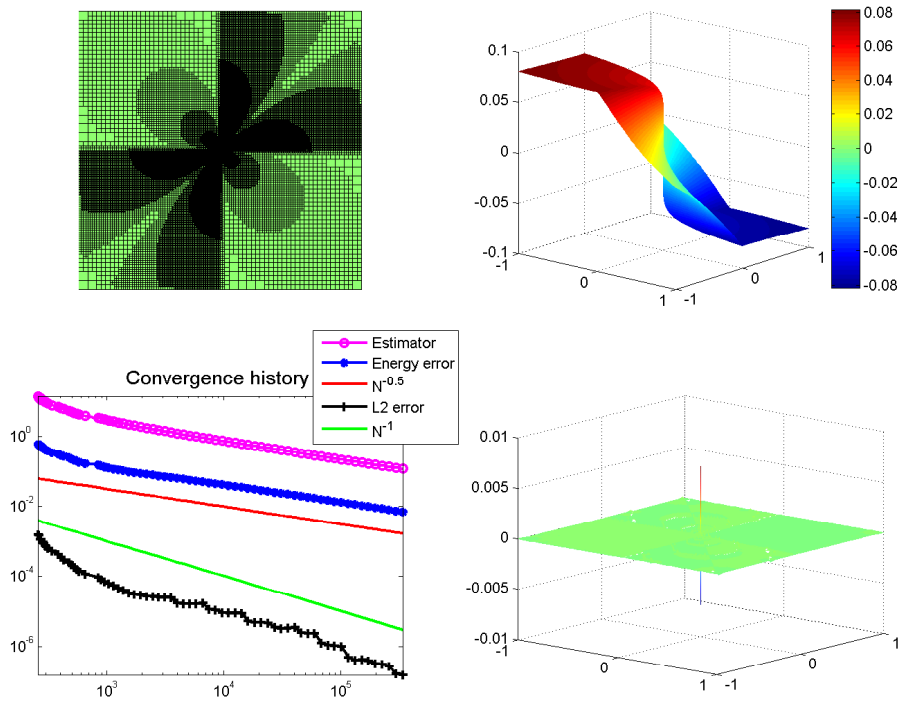


Fig. 5.5. The performance of algorithm $\mathcal{AFEM}$ with original error estimator: (Top left) The final mesh with 338851 elements; (Bottom left) Convergence history with the parameter $\theta = 0.5$; (Top right)The surface plot of the final discrete solution $u_h$ with 338851 elements; (Bottom right) The surface plot of the relative error $(u - u_h)/\|u\|_{L^\infty(\Omega)}$ of the final discrete solution $u_h$ with 338851 elements and the maximum of the relative error is 0.0069.

**Example 5.3.** (***Kellogg problem***) *We choose the following elliptic problem with piecewise constant coefficients and vanishing right-hand side $f$ to compute. Let $\Omega = (-1,1)^2$, $\boldsymbol{A} = RI$ in the first and third quadrants, and $\boldsymbol{A} = I$ in the second and fourth quadrants, where $R$ is a constant to be given later. Consider the following problem*

$$-div(\boldsymbol{A}\nabla u) = 0, \ \ in\ \Omega \quad \ and \quad \ u = g_D \ on\ \partial\Omega.$$

*We choose $g_D$ to fit the exact solution $u$ which is given in polar coordinates by $u(r,\phi) = r^\tau \mu(\phi)$, where*

$$\mu(\phi) = \begin{cases} \cos((\frac{\pi}{2} - \sigma)\tau) \cdot \cos((\phi - \frac{\pi}{2} + \rho)\tau), & if \ \ 0 \le \phi \le \frac{\pi}{2}, \\ \cos(\rho\tau) \cdot \cos((\phi - \pi + \sigma)\tau), & if \ \ \frac{\pi}{2} \le \phi \le \pi, \\ \cos(\sigma\tau) \cdot \cos((\phi - \pi + \rho)\tau), & if \ \ \pi \le \phi \le \frac{3\pi}{2}, \\ \cos((\frac{\pi}{2} - \rho)\tau) \cdot \cos((\phi - \frac{3\pi}{2} - \sigma)\tau), & if \ \ \frac{3\pi}{2} \le \phi \le 2\pi. \end{cases}$$

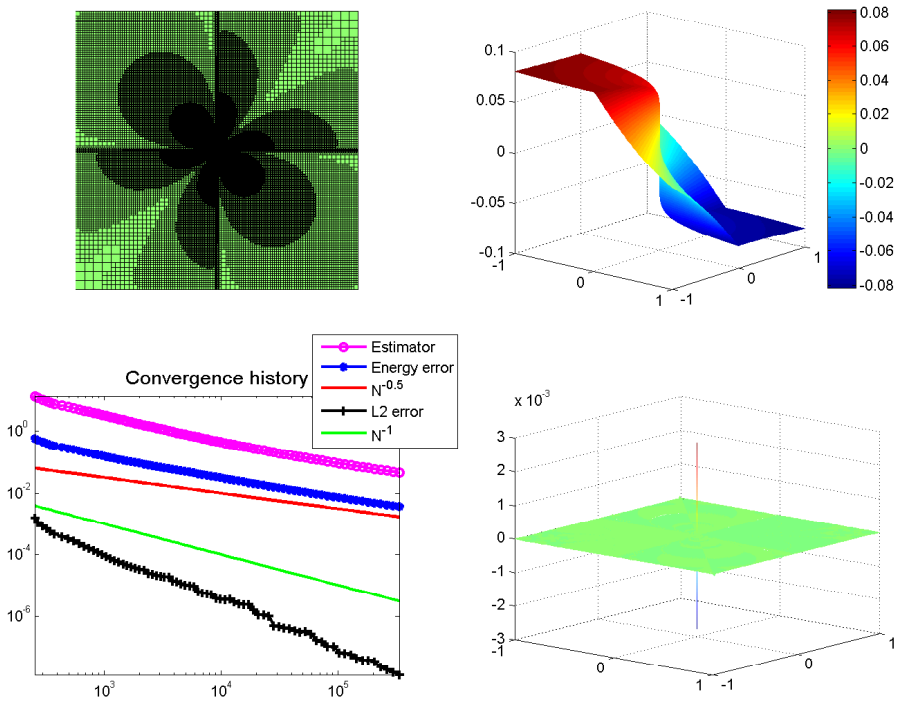


Fig. 5.6. The performance of algorithm $\mathcal{AFEM}$ with modified error estimator: (Top left) The final mesh with 333433 elements; (Bottom left) Convergence history with the parameter $\theta = 0.9$; (Top right) The surface plot of the final discrete solution $u_h$ with 333433 elements; (Bottom right) The surface plot of the relative error $(u - u_h)/\|u\|_{L^\infty(\Omega)}$ of the final discrete solution $u_h$ with 333433 elements and the maximum of the relative error is 0.0028.

*and the numbers* $\tau, \rho, \sigma$ *satisfy the nonlinear relations*

$$\begin{cases} R = -\tan((\frac{\pi}{2} - \sigma)\tau) \cdot (\rho\tau), \\ 1/R = -\tan(\rho\tau) \cdot \cot(\sigma\tau), \\ R = -\tan(\sigma\tau) \cdot \cot(\frac{\pi}{2} - \rho)\tau), \\ 0 < \tau < 2, \\ \max\{0, \pi\tau - \pi\} < 2\tau\rho < \min\{\pi\tau, \pi\}, \\ \max\{0, \pi - \pi\tau\} < -2\tau\sigma < \min\{\pi\tau, 2\pi - \pi\tau\}. \end{cases} \tag{5.15}$$

*The solution* $u$ *is in* $H^{1+s}$ *with* $s < \tau$. *For* $\tau = 0.1$, *solving the above nonlinear equation* (5.15) *yields*

$$R \approx 161.4476387975881, \quad \rho = \frac{\pi}{4}, \quad \sigma \approx -14.92256510455152.$$

We firstly solve this problem with the a posteriori error estimator (4.8). The four pictures in Figure 5.5 are the final mesh with 338851 elements, the corresponding discrete solution $u_h$, the convergence history with $\theta = 0.5$ and the relative error $(u - u_h)/\|u\|_{L^\infty(\Omega)}$ with 338851 elements respectively.

Second, we solve this problem with a modified posteriori error estimator which reads:

$$\widetilde{\eta}_\ell^2(v,K) := h_K^2 \parallel \widetilde{R}_K(v) \parallel_{L^2(K)}^2 + h_K \parallel \widetilde{J}(v) \parallel_{L^2(\partial K \cap \Omega)}^2, \quad \forall K \in \mathcal{T}_\ell, \tag{5.16}$$

where

$$\widetilde{R}_K(v) := \Lambda_K^{-\frac{1}{2}}(f + \Delta v)|_K, \ \forall K \in \mathcal{T}_\ell,$$
$$\widetilde{J}(v)|_E := \Lambda_E^{-\frac{1}{2}}([\![\mathbf{A}\nabla v]\!] \cdot \nu_E)|_E, \ \forall E \in \mathcal{E}_0,$$

and

$$\Lambda_K := \min_{K' \in \Omega_K} (\mathbf{A}|_{K'}) \quad \text{and} \quad \Lambda_E := \min_{K' \in \Omega_E} (\mathbf{A}|_{K'}).$$

For this modified estimator, one can show that

$$\|\mathbf{A}^{\frac{1}{2}}\nabla(u - u_\ell)\|_{0,\Omega}^2 \le C_5 \widetilde{\eta}_\ell^2(u_\ell, \mathcal{T}_\ell), \tag{5.17}$$

where $C_5$ is a constant dependent only on the shape regularity of mesh $\mathcal{T}_\ell$.

The four pictures in Figure 5.6 are the final mesh with 333433 elements, the corresponding discrete solution $u_h$, the convergence history with $\theta = 0.9$ and the relative error $(u - u_h)/\|u\|_{L^\infty(\Omega)}$ with 333433 elements respectively. The maximum of the relative error using this modified estimator on the final mesh with 333433 elements is 0.0028 while the maximum of the relative error using this original estimator on the final mesh with 338851 elements is 0.0069. Obviously, the modified error estimator (5.16) can capture the singularity more efficiently and lead to a better result.

## 6. Conclusion

In this paper we proved the convergence of adaptive conforming $\mathbb{Q}_m$ element methods on general quadrilateral and hexahedral 1-irregular meshes. The implementations verified our theoretical findings. In our future work, we will extend our results to adaptive mixed and nonconforming quadrilateral FEMs [27, 28], where new difficulties are involved and new techniques need to be developed.

**Acknowledgments.** The research is supported by the Special Funds for Major State Basic Research Project (No. 2005CB321701).

## References

[1] M. Ainsworth, J.T. Oden, A posteriori error estimation in finite element analysis, Pure and Applied Mathematics, Wiley-Interscience, John Wiley Sons, New York, 2000.

[2] I. Babuska, W.C. Rheinboldt, Error estimates for adaptive finite element computations, *SIAM J. Numer. Anal.,* **15** (1978), 736-754.

[3] R. Becker, S. Mao, Z.C. Shi, A convergent adaptive finite element method with optimal complexity, *Electron. T. Numer. Anal.,* **30**(2008), 291-304.

[4] R. Becker, S. Mao, An optimally convergent adaptive mixed finite element method, *Numer. Math.,* **111** (2008), 35-54.

[5] S.C. Brenner, L.R. Scott, The Mathematical Theory of Finite Element Methods, Springer Verlag, 2nd ed., 2002.

[6] C. Carstensen, Jun Hu, Hanging nodes in the unifying theory of a posteriori finite element error control, *J. Comput. Math.,* **27** (2009), 215-236.

[7] C. Carstensen, R.H.W. Hoppe, Error reduction and convergence for an adaptive mixed finite element method, *Math. Comput.,* **75** (2006), 1033-1042.

[8] C. Carstensen, R.H.W. Hoppe, Convergence analysis of an adaptive nonconforming finite element methods, *Numer. Math.,* **103** (2006), 251-266.

[9] J.M. Cascon, Ch. Kreuzer, R.N. Nochetto, K.G. Siebert, Quasi-optimal convergence rate for an adaptive finite element method, *SIAM J. Numer. Anal.,* **46** (2008), 2524-2550.

[10] H.X. Chen, X.J. Xu, R.H.W. Hoppe, Convergence and Optimality of Adaptive Nonconforming Finite Element Methods for Nonsymmetric and Indefinite Problems, Submitted, (2008).

[11] L. Chen, M. Holst, J.C. Xu, Convergence and optimality of adaptive mixed finite element methods, *Math. Comput.,* **78** (2009), 35-53.

[12] Z. Chen, S. Dai, On the efficiency of adaptive finite element methods for elliptic problems with discontinuous coefficients, *SIAM J. Sci. Comput.*, **24** (2002), 443-462.

[13] P.G. Ciarlet, The Finite Element method for Elliptic Problems, Amsterdam, North-Holland, 1978.

[14] R.W. Clough and J.L. Tocher, Finite element stiffness matrices for analysis of plates in bending, Proceedings of the Conference on Matrix Methods in Structural Mechanics, Wright-Patterson A.F.B., Ohio (1965), 515-545.

[15] W. Dörfler, A convergent adaptive algorithm for Poisson's equation, *SIAM J. Numer. Anal.,* **33** (1996), 1106-1124.

[16] L.C. Evans, Partial Differential Equations, American Mathematical Society Providence, Rhode Island, 1998.

[17] V. Girault and P.A. Raviart, Finite element methods for Navier-Stokes equations, Theory and Algorithm, Springer, Berlin, 1986.

[18] P. Grisvard, Elliptic Problems in Nonsmooth Domains, Pitman, Boston, 1985.

[19] V. Heuveline, F. Schieweck, $H^1$ -interpolation on quadrilateral and hexahedral meshes with hanging nodes, *Computing,* **80** (2007), 203-220.

[20] K. Mekchay, R.H. Nochetto, Convergence of adaptive finite element methods for general second order linear elliptic PDE, *SIAM J. Numer. Anal.,* **43** (2005), 1803-1827.

[21] P. Morin, R.H. Nochetto, K.G. Siebert, Data oscillation and convergence of adaptive FEM, *SIAM J. Numer. Anal.,* **38** (2000), 466-488.

[22] P. Morin, R.H. Nochetto, K.G. Siebert, Convergence of adaptive finite element methods, *SIAM Rev.,* **44** (2002), 631-658.

[23] A.H. Schatz, An observation concerning Ritz-Galerkin methods with indefinite bilinear forms, *Math. Comput.,* **28** (1974), 959-962.

[24] L.R. Scott and S.Y. Zhang, Finite element interpolation of nonsmooth functions satisfying boundary conditions, *Math. Comput.,* **54** (1990), 483-493.

[25] Z.C. Shi, A convergence condition for the quadrilateral Wilson element, *Numer. Math.,* **44** (1984), 349-361.

[26] R. Verfürth, A Review of a Posteriori Error Estimation and Adaptive Mesh-Refinement Techniques, Wiley-Teubner, Chichester, 1996.

[27] X.Y. Zhao, S.P. Mao, Z.C. Shi, Convergence and quasi-optimality of adaptive mixed element methods, 2009, preprint.

[28] X.Y. Zhao, S.P. Mao, Z.C. Shi, Optimal convergence of adaptive rotated $Q_1$ finite element methods, 2009, preprint.